

Surprising Variability of the Planetary Nebula IC 4997=QV Sge

V.P. Arkhipova, M.A. Burlak*, N.P. Ikonnikova, G.V. Komissarova,
V.F. Esipov, V.I. Shenavrin

*Sternberg Astronomical Institute,
Moscow State University (SAI MSU), Universitetskii pr. 13, Moscow, 119992 Russia*

We present the results of a new epoch (2009-2019) of a long-term (50 years) photometric monitoring of the variable planetary nebula IC 4997 (QV Sge). The integral (star + nebula) UBV light curves display a continuing brightening of $0.^m15$ in V , a slight rise ($<0.^m1$) in B , and constancy in U . The $B - V$ color has got redder from $0.^m4$ in 2000 to $0.^m7$ in 2019, whereas the $U - B$ color has not changed significantly at that time. We carried out near infrared (IR) $JHKL$ photometry in 2019, and comparing it to the data obtained in 1999-2006 we found the source to be fainter by $0.^m4$ in L and bluer by $0.^m2$ in the $K - L$ color. The long-term brightness variations in the optical and IR regions are shown to be due mostly to the changing input of emission lines to the integral light.

Low-dispersion spectroscopic observations carried out in 2010-2019 revealed a continuing decrease in the [OIII] $\lambda 4363$ to $H\gamma$ intensity ratio: it decreased by a factor of ~ 3 in 30 years and reached the level of 1960-1970. We discovered that the absolute intensities of [OIII] $\lambda 4959$ и $\lambda 5007$ nebular lines had increased by a factor of > 2 from 1990 to 2019, whereas the [OIII] $\lambda 4363$ auroral line had weakened by a factor of 2 comparing to the maximum value observed in 2000. The variation of $H\beta$ absolute intensity in 1960-2019 was shown to be similar to that of [OIII] $\lambda 4959$ (and $\lambda 5007$), but of smaller amplitude. The electron density in the outer part of the nebula was estimated from the [SII] and [CIII] lines. Basing on the data on absolute intensities for the $H\beta$, [OIII] $\lambda 4363$, 4959 lines and their ratios we propose a possible scenario describing the change of physical conditions (N_e, T_e) in IC 4997 in 1970-2019. The main features of spectral variability of IC 4997 could be explained by a variation of electron temperature in the nebula caused by not so much the change in ionizing flux from the central star as the variable stellar wind and related processes. The photometric and spectral changes observed for IC 4997 in 1960-2019 may be interpreted as an observable consequence of a single episode of enhanced mass loss from the variable central star.

Keywords: *planetary nebulae, photometric and spectral variability, IC 4997, QV Sge, gas shell diagnostics, electron temperature, electron density.*

*E-mail: marina.burlak@gmail.com

INTRODUCTION

IC 4997 attracted particular attention as the first confirmed variable source of radiation among the young planetary nebulae (PNs). Liller and Aller (1957) reported a noticeable change in the $\lambda 4363$ [OIII] to $H\gamma$ intensity ratio, having compared their own spectral measurements of 1956 with those of Menzel et al. (1941) made in 1938. Vorontsov-Velyaminov (1960) confirmed the variability of the ratio basing on the spectra obtained in Crimea in 1959-1960.

IC 4997 received a great deal of interest in the 1960-1970s: the spectrophotometric observations were carried out by O'Dell (1963), Aller and Kaler (1964), Aller and Liller (1966), - and later by Ferland (1979), Feibelman et al. (1979), Purgathofer (1981). The optical spectrum of IC 4997 was the most thoroughly investigated in Hyung et al. (1994), Hyung and Aller (1993), where the relative intensities of more than 500 emission lines in the $\lambda\lambda 3647 - 10049$ region were measured in the echelle spectra obtained in 1990 and 1991. The authors also noted the change in relative fluxes for quite a number of other emission lines besides [OIII] $\lambda 4363$ and $H\gamma$ over a year of high-dispersion observations.

A large infrared (IR) excess in the $11 \mu\text{m}$ range was first detected for IC 4997 by Gillett et al. (1971). Natta and Panagia (1981), Pottasch et al. (1984), Lenzuni et al. (1989) thoroughly studied the IR spectrum of the nebula and its dust envelope. Basing on IR photometry carried out in 1999-2006 Taranova and Shenavrin (2007) found the variability of IC 4997 with a peak-to-peak amplitude of $0.^m20-0.^m25$ in H and $0.^m05$ in J .

Radio observations carried out by Miranda et al. (1996), Miranda and Torrelles (1998) made it possible to construct for IC 4997 a map of 3.6 cm and 2 cm continuum radiation with angular resolution better than $0.''1$. The authors described new details in the structure of its outer and inner shells and confirmed the double-shell model for the nebula suggested previously by Hyung et al. (1994). Investigating the variability of IC 4997 radio flux Miranda and Torrelles (1998) found short timescale (< 1 year) morphological changes in the inner shell structure in the vicinity of the central star $< 0.3''$ and explained them by the collimated stellar wind impinging on the outer shell of the nebula. According to the archival data, the 5 GHz radio flux from the optically thin part of the nebula has decreased from 100 mJy around 1989 (Acker et al., 1992) to 45 mJy in 1996 (Gómez et al., 2002). Subsequent observations (Casassus et al., 2007, Pazderska et al., 2009) showed an increase in radio flux from 80 to 108 mJy at a frequency of 30 GHz but the data was not enough to analyze the radio spectrum in detail.

The central star of IC 4997, HD 193538=QV Sge, was classified in a number of papers as a weak emission line star – *wels*. It's hard to divide the observed integral optical spectrum into the components belonging to the nebula and the central star, but the CIV $\lambda 5801$, 5812 and CIII $\lambda 4650$ emission lines are identified in the echelle spectra with confidence and assigned to the star regarding their width (Hyung et al., 1994, Marcolino and de Araújo, 2003). Marcolino et al. (2007) noted that the CIV $\lambda 1549$ emission line was not in a P Cyg feature in the SWP 31683 spectrum (1987-09-01) taken from the IUE archive but analyzing an earlier IUE spectrum SWP 08578 (1980-03-27) they could see some difference: a slightly higher continuum and the NV $\lambda 1238$ line possibly in a P Cyg feature in the earlier spectrum. The authors concluded that such profiles are formed in the stellar wind of the central star and not in the nebula. This fact may imply the variability of the IC 4997 central star related to the existence of a variable stellar wind.

According to the Sahai et al. (2011) morphological classification system, IC 4997 was assigned to bipolar PN regarding its Hubble Space Telescope image. The bright part of the nebula extends to $< 2''$ from the central star and consists of two pairs of diametrically opposed lobes whose axes are perpendicular one to another.

Regular *UBV* photometric and spectral observations of IC 4997 at the Crimean astronomical station (CAS) of SAI MSU were initiated by E.B. Kostyakova and started in 1968. The angular

visible size of the nebula is about $2''$. Both photometric and spectral observations realized as part of the program include the whole nebula together with the central star HD 193538. The results of photometric and spectral monitoring in different epochs were published in a quite number of papers: Vorontsov-Velyaminov et al. (1970), Kostyakova (1971), Kostyakova et al. (1973), Arkhipova et al. (1994), Kostyakova (1990, 1999), Kostyakova and Arkhipova (2009), Burlak and Esipov (2010). We continue observing IC 4997 on the CAS telescopes and in this paper we analyze the measurements obtained in 2009-2019 together with previous data.

OBSERVATIONS

UBV photometry

Although there is a good deal of single integral brightness estimates for IC 4997 published, it would hardly make sense to compare them as there are many strong emissions and the photometric systems are slightly different, which leads to a significant scatter in data. We succeeded to maintain a long-term monitoring at the same telescope with permanent equipment.

Our *UBV* observations of IC 4997 have been carried out with the photon counting photometer constructed by Lyutyi (Lyutyi, 1971) mounted at the Cassegrain focus of the Zeiss-600 telescope of CAS since 1971. Previous results obtained mainly by Kostyakova E.B. can be found in Kostyakova et al. (1973), Kostyakova (1991), Arkhipova et al. (1994), Kostyakova and Arkhipova (2009). In this paper we present recent *UBV* photometry obtained in 2009-2019. As usual, HD 355464 was used as a reference star, and its magnitudes ($V = 9.^m98$, $B = 10.^m08$, $U = 10.^m10$) were acquired via referencing to photometric standards in NGC 6633 and NGC 7063 (Hiltner et al., 1958). The standard errors in the photometric magnitudes are $\sigma_V = 0.^m009$, $\sigma_B = 0.^m009$, $\sigma_U = 0.^m012$. The measurements were carried out with an aperture of $27''$ (sometimes $13''$), so we measured the integral brightness of the object – the PN and the central star.

Here we present the magnitudes in the instrumental system which is very close to the standard one of Johnson. Standard data reduction procedures were performed, and besides, the magnitudes were reduced to the common under-dome temperature ($t = +10^\circ\text{C}$) and a correction was introduced after a slight change of instrumental system in 1989 when the photomultiplier was substituted.

The magnitude – temperature relations for B and V can be expressed by the equations:

$$\Delta V = 0.121 - 0.013t + 1.624 \times 10^{-4}t^2, \Delta B = -0.011 - 0.001t, \quad (1)$$

where t is the under-dome temperature in Celsius degree.

To reduce new data to the previous photometric system we introduce the following corrections: $\Delta V = 0.^m109$, $\Delta B = -0.^m084$, $\Delta U = -0.^m040$.

In Table 1 we present *UBV* photometry for IC 4997 obtained in 2009-2019. To analyze its long-term variability we calculated the annual average *UBV* magnitudes and present them in Table 2 together with standard deviation (σ) and number of observations (N).

IR photometry

We carried out IR photometric monitoring at the 1.25-m telescope of CAS in 1999-2006 and resumed in 2019. The photometer with a liquid nitrogen cooled photovoltaic indium antimonide (InSn) detector installed at the Cassegrain focus was used. The output aperture was $\approx 12''$, the spatial separation of the beams during modulation was $\approx 30''$ in the east–west direction. The star BS 7635 from Johnson et al. (1966) was used as a photometric standard. The results of IR monitoring in 1999-2006 were published in Taranova and Shenavrin (2007). New *JHKL* magnitudes obtained in 2019 are listed in Table 3.

Spectral observations

Optical spectroscopy of IC 4997 was carried out at the 1.25-m telescope of CAS in 2010-2019. We used a low-dispersion spectrograph with a $600 \text{ lines mm}^{-1}$ grating. The detector was a ST-402 CCD 765×510 pixels in size. The slit width was constant and equal to $4''$. The spectral resolution obtained was near 7.4 \AA as measured from the fullwidth half maximum (FWHM). The spectrograph configuration was different in August and October, 2019: the spectra were obtained with another camera objective lens and a FLI PL-4022 CCD 2048×2048 pixels in size. A binning of 2×2 was used, obtaining nearly the similar spectral resolution as before. For flux calibration spectrophotometric standard stars with known spectral energy distribution were also observed: 107 Her, 18 Vul, 29 Vul, HD 196775, 40 Cyg, ρ Aql (Glushneva et al., 1998; Pickles, 1998). The standard stars were observed before or after IC 4997 at close airmasses. We show the log of observations in Table 4.

Due to the spectrograph design it's possible to obtain simultaneously a part of spectrum of $\sim 1500 \text{ \AA}$ or $\sim 2400 \text{ \AA}$ in the previous or new configuration respectively. To cover the whole observable wavelength range ($\sim 4000\text{--}9500 \text{ \AA}$) it's necessary to obtain 4 or 3 overlapping frames. Usually the airmass difference between IC 4997 and the standard star did not exceed 0.2. Under stable atmospheric conditions the estimated error in the absolute flux calibration was about $\sim 5\%$, as is was indicated by good matching of overlapping parts of spectra. Under non-stable conditions the calibration error increased (up to 20%).

To measure the emission line intensities we integrated all the flux in the line. Table 5 presents observed relative emission line intensities on the scale $I(\text{H}\beta) = 100$, and the observed flux $F(\text{H}\beta)$ in absolute units. For the lines brighter than 1% of the $\text{H}\beta$ line the estimated error is about 10%, and about 25% for the weaker ones.

In order to examine the physical conditions in the nebula, we had to correct the relative intensities for the interstellar reddening. Burlak and Esipov (2010) reviewed the previous attempts to determine the reddening coefficient for IC 4997, and using their spectral data obtained in 2003–2009 they derived $c(\text{H}\beta) = 0.35$ taking into account self-absorption in the hydrogen lines. Our new spectral data agree well enough with this value of $c(\text{H}\beta)$. It's worth mentioning that the Balmer decrement was indicative of self-absorption in 2010–2019, too, but the effect seems to have weakened by 2019.

PHOTOMETRIC VARIABILITY

The integral brightness of IC 4997 varies with a typical seasonal range of less than $0.^m2$ and demonstrates a long-term trend over the last 50 years. Figure 1 shows the evolution of the annual average UBV brightness, and $U - B$, $B - V$ color indices in 1968–2019 basing on the results of Kostyakova et al. (1973), Kostyakova (1991, 1999), Arkhipova et al. (1994), Kostyakova and Arkhipova (2009), unpublished measurements of E.B. Kostyakova and new data.

The variation of the annual average magnitude appears to have an amplitude of $0.^m6$ in V , $0.^m4$ in B , and about $0.^m3$ in U . Note that in 50 years of our monitoring the integral U and B magnitudes described a gradual asymmetric curve and returned to the initial state, while the V brightness continued to increase after 2010, and the object is $0.^m2$ brighter at present than it was when we started observing it. The $B - V$ and $U - B$ color indices varied less gradually and appeared bluer and with larger scatter when the object was fainter that could be ascribed to the effect of variable emission lines.

To estimate the input from emission into the UBV brightness we isolated the emission nebular component of IC 4997 from the average UBV magnitudes for the year 1990 using the most complete and reliable spectral data for this year from Hyung et al. (1994). We took into account the lines not fainter than 0.05 on the scale $I(\text{H}\beta) = 100$. Unfortunately, the given paper contains only relative line intensities for IC 4997 in August, 1990. The data were flux-calibrated using the absolute measurement

of $H\beta$ intensity in 1990 made by Kostyakova and Arkhipova (2009): $F(H\beta) = 2.6 \times 10^{-11} \text{erg cm}^{-2} \text{s}^{-1}$. We calculated the averaged values of brightness and color over 12 estimates obtained in May-October, 1990: $V = 11.^m07$, $B = 11.^m52$, $U = 10.^m98$, $B - V = +0.45$, $U - B = -0.54$. The input from emission lines was estimated using the passbands of our UBV instrumental system.

Note that photometric and spectrophotometric observations were carried out at different nights, the averaged date of all measurements falls on the end of July, 1990.

So, we estimated the emission lines input into the UBV brightness, and calculated the integral continuum flux and magnitude for the object in 1990.

$$\begin{aligned} F_V(\text{lines}) &= 4.57 \times 10^{-11} \text{erg cm}^{-2} \text{s}^{-1}, F_V(\text{cont}) = 8.91 \times 10^{-11} \text{erg cm}^{-2} \text{s}^{-1}, V(\text{cont}) = 11.^m51; \\ F_B(\text{lines}) &= 11.06 \times 10^{-11} \text{erg cm}^{-2} \text{s}^{-1}, F_B(\text{cont}) = 4.73 \times 10^{-11} \text{erg cm}^{-2} \text{s}^{-1}, B(\text{cont}) = 12.^m83; \\ F_U(\text{lines}) &= 2.35 \times 10^{-11} \text{erg cm}^{-2} \text{s}^{-1}, F_U(\text{cont}) = 17.11 \times 10^{-11} \text{erg cm}^{-2} \text{s}^{-1}, U(\text{cont}) = 11.^m14. \end{aligned}$$

The emission lines input into the UBV integral brightness of the variable PN IC 4997 in 1990 was as large as 30 % in V , 70 % in B , and more than 13 % in U (since no emission lines were measured beyond the Balmer discontinuity in 1990).

We'd like to highlight the input of the [OIII] nebular lines $\lambda 5007$, $\lambda 4959$ and $H\beta$ into the B and V integral light. In Figure 2, we present the relationship between the summary flux from $H\beta$, [OIII] $\lambda 4959$, $\lambda 5007$, which dominate the blue region, and the annual average V and B brightness in 1972-2019. It is clearly seen that the summary flux from these three lines $\lg(F(H\beta) + F(\lambda 4959) + F(\lambda 5007))$ and the V and B brightness are closely related: the correlation coefficients are 0.90 and 0.81 respectively. Therefore, the B and V photometric variability may be explained by the changing emission spectrum of the nebula. Similar analysis for the U band is complicated by the absence of data on the changes of nebular spectrum in the wavelength range bluer than $\lambda 3700$.

The color indices for the summary continuum of the nebula and central star appeared to be $B - V = +1.^m32$, $U - B < \sim 1.^m69$. Assuming $E(B - V) = 0.^m24$ for IC 4997, we got the reddening corrected color indices for the summary continuum: $(B - V)_0 = +1.^m08$, $(U - B)_0 < \sim 1.^m89$.

The emission lines input having been removed, the position of IC 4997 in the color-color diagram appears to be similar to that of a hot star with a temperature more than 35000 K and a rather optically thick gas continuum. We estimate the position uncertainty associated with the mismatching of dates of photometric and spectral observations to be equal to $\sim 0.^m3$.

Note that IC 4997 was undoubtedly classified as a bipolar PN (Sahai et al., 2011). The bipolar PNs which have an hourglass-like morphology (i.e. a cylinder with a 'pinched-in' shape in the region around the center) are now widely considered to have a binary central star. And in this regard, we were interested to find some traces of the possible central star binarity in the summary optical continuum. The color indices $(B - V)_0(\text{cont}) = 1.08$ and $(U - B)_0(\text{cont}) < -1.89$ resulted from subtracting the emission lines input and reddening correction demonstrate a slight red excess in the $(B - V)$ color which is not reliable due to low accuracy.

IC 4997 displays a variation in IR brightness, too. Taranova and Shenavrin (2007) basing on the $JHKL$ photometry made in 1999-2006 showed that the amplitude of variation in $JHKL$ was nearly $0.^m2 - 0.^m3$ and that in the $J - H$, $H - K$ и $K - L$ colors was up to $\sim 0.^m5$ within a characteristic time of 260-280 days. The authors suggested that the detected variation in H was associated with the changing input of the hydrogen Brackett lines. In 2019 we carried out the observations of IC 4997 with the same equipment as had been used previously. In Figure 3 we present the near IR light and color curves for IC 4997 compiled from the data published by Taranova and Shenavrin (2007) and the new measurements obtained in 2019. As is seen from the figure, the H and K brightness in 2019 is at the level of the minimum values for the 1999-2006 interval, whereas the average J brightness has decreased by $0.^m25$. The most prominent change is seen for the L band: the brightness has decreased by $0.^m4$. The color indices have barely changed on average since 1999 and are about $J - H = -0.^m2$, $J - K = 0.^m5$, $H - K = 0.^m7$, only the $K - L$ color has decreased from $1.^m5$ to $1.^m3$.

Whitelock (1985) reviewed the principal sources of near IR emission for PNs: they are the free-free and free-bound radiation of hydrogen and helium plasma and the thermal emission from dust with $T_d > 1000$ K (if there is dust in the nebula). There is also a small input of the central star and a significant one from the emission lines, the strongest ones being:

J band: $P\beta$, $P\gamma$, He II $\lambda 1.162\mu\text{m}$, He I $\lambda 1.083\mu\text{m}$;

H band: Brackett series from Br 10 $\lambda 1.737\mu\text{m}$ to nearly the series limit at $\lambda 1.459\mu\text{m}$;

K band: $\text{Br}\gamma$ and He I $\lambda 2.058\mu\text{m}$.

Whitelock (1985) proposed a classification scheme for PNs based on the major source of 1-2 μm emission and assigned IC 4997 to the N (Nebula) group due to the nebula radiation dominating the near IR domain. Note that IC 4997 is a PN of low excitation, so the He II $\lambda 1.162\mu\text{m}$ is not present in the spectrum. Thus, trying to explain the *JHK* variability of IC 4997 we can ignore the impact of the dust component and consider the change in intensities of H I and, to a lesser degree, of He I lines responsible for variation.

Ohsawa et al. (2016) presented near IR (2.5–5.0 μm) spectra for 72 PNs including IC 4997 obtained with IRC/AKARI. Due to this work, we have an idea of the most important emission lines of IC 4997 falling into the *L* passband: they are $\text{Br}\alpha$ $\lambda 4.05\mu\text{m}$ and $\text{Br}\beta$ $\lambda 2.62\mu\text{m}$. Therefore, the *L* brightness variability of IC 4997 may relate to the change in the intensity of these lines.

SPECTRAL VARIABILITY

The change in the intensity ratio of the lines [OIII] $\lambda 4363$ and $\text{H}\gamma$ was the first evidence for the spectral variability of IC 4997 due to the fact that it could be easily measured with confidence. In Figure 4 we reconstruct the long-term (several decades) evolution of the $F(\lambda 4363)/F(\text{H}\gamma)$ ratio basing on the data from this work and the previous estimates made by different researchers since 1938: Aller (1941), Struve and Swings (1941), Page (1942), White (1952), Liller and Aller (1963), Aller and Liller (1966), Vorontsov-Velyaminov et al. (1965), Aller and Kaler (1964), O’Dell (1963), Ahern (1978), Feibelman et al. (1979), Purgathofer (1978), Purgathofer and Stoll (1981), Acker et al. (1989), Hyung et al. (1994), Kostyakova and Arkhipova (2009). Besides, we have estimated line intensities in the spectrum of IC 4997 published by Hajduk et al. (2015) and in another one found in the HASH PN database (Parker et al., 2016). Over the entire period of observations the ratio has described a wave with a peak-to-peak amplitude of 0.45 in the logarithmic scale and a characteristic time of 50-60 years. The $\lambda 4363/\text{H}\gamma$ ratio continued to decrease in 2010-2019 following the trend set around 1990, and by 2019 the ratio has reached the value observed in 1960–1970.

In addition to the variation of $F(\lambda 4363)/F(\text{H}\gamma)$, the nebular [OIII] lines intensities relative to $\text{H}\beta$ were found to vary, too. Since 1960–1970 their intensities at first decreased until 1985, then they grew to 2005, and since then they stay at the approximately constant level slightly higher than that of the early sixties. Note that the relative intensities of the nebular and auroral lines have changed differently which is well illustrated by Figure 5. There is also a hint of variability in He I lines but the data are less reliable and available for a smaller time interval. In Figure 5 we present the evolution of the He I $\lambda 5876$ intensity relative to $\text{H}\beta$: in general, the change was inverse to that of the nebular lines (Vorontsov-Velyaminov et al., 1965; O’Dell, 1963; Aller and Walker, 1970; Ahern, 1978; Acker et al., 1989; Hyung et al., 1994; Hajduk et al., 2015; Parker et al., 2016). The He I $\lambda 6678$ line varies in a similar way to $\lambda 5876$, at least since 1986 – we have not managed to find earlier measurements for the $\lambda 6678$ line.

Figure 6 shows the observed absolute intensities for the [OIII] $\lambda 4363$, $\lambda 4959$ lines measured by different researchers over the last 60 years. Although there is a big scatter in estimates for these lines, the trend is well defined. Since 1960 the absolute intensity of the auroral line grew at an approximately constant rate, reached maximum level about 2000–2005 having increased more than twice, and then

started to decrease faster than it had been increasing. Since 1960 the absolute intensities of nebular lines stayed quite constant with a possible slight tendency to decrease, but in the mid-1970s dropped sharply and reached minimum level around 1985-1990, then increased at a lower rate to the values observed about 1960 or little higher, thereby having reproduced the optical light curve of IC 4997.

It would be interesting to ascertain whether the absolute intensity of $H\beta$ varies, but the absolute spectrophotometry is very difficult to perform, and there are inconsistencies between observers which produce large scatter in data constituting definite obstruction to the determination of the shape and characteristic parameters of the $H\beta$ intensity variation. Nevertheless, one can see a period of higher absolute intensity before 1980, then it faded by 30% and stayed more or less constant until 2000-2005, and after that started to grow.

As regards the variability of other lines, it's worth mentioning that mostly short wave region of optical spectrum was investigated in earlier epochs, while the long wave one – later. So, just several lines were measured over a long-term period, and only for a few the estimates are reliable. Figure 7 shows the evolution of relative intensities for the [SIII] $\lambda 6312$ and [NII] $\lambda 5755$ auroral lines, and the [ArIII] $\lambda 7135$ nebular line. In 1986-2019 [SIII] $\lambda 6312$ reproduced the behavior of the [OIII] auroral line, its relative intensity decreased, whereas the variation of [NII] $\lambda 5755$ was inverse to that of [OIII] $\lambda 4363$. We have not managed to ascertain the change in [ArIII] $\lambda 7135$ relative intensity over the given time interval.

DIAGNOSTICS AND PHYSICAL PARAMETERS OF THE IC 4997 NEBULA

"One has to be an optimist to attempt to construct
a model for IC 4997..."
(Huyng, Aller, Feibelman, 1994)

After the variability of the $F(\lambda 4363)/F(H\gamma)$ and $F(\lambda 4363)/F(\lambda 4959 + \lambda 5007)$ ratios was discovered and till about 1970, some suggestions were proposed to explain these spectral changes. Gurzadian (1958), Vorontsov-Velyaminov (1960) and Khromov (1962) considered the fall in the central star temperature to be the cause of the decrease in $F(\lambda 4363)/F(H\gamma)$, though Gurzadian believed this change in temperature to be of an evolutionary character, Vorontsov-Velyaminov – to have a long periodic nature, Khromov – to be oscillatory fluctuations. According to Aller and Liller (1966), the spectral changes resulted from the expansion of the nebula with a corresponding decrease both in electron density and electron temperature. In addition to long-term changes, fast oscillations of the $F(\lambda 4363)/F(H\gamma)$ ratio within one year were detected, and Ferland (1979) supposed that they were due to the variation of electron temperature attributed to small changes in the number of ionizing photons emitted by the central star: since the electron density is high in the inner parts of the nebula ($N_e \sim 10^6 \text{ cm}^{-3}$) where the [OIII] $\lambda 4363$ line is mostly generated, the thermal equilibrium is set very quickly and a well-defined temperature will always be present. Although there is a variety of diagnostic ratios measured for IC 4997 in the optical and ultraviolet regions, the constructing of a quantitative model turned out to be a difficult task, especially if one aims not only to describe the instantaneous state of the nebula and central star but also to interpret its change (see Hyung et al., 1994 for more detail). Various ions emit in different zones and there exists a large range in electron density and temperature for them. So, the region of intersection of all the curves corresponding to different ions encompasses a large range of N_e, T_e values in the diagnostic diagram for IC 4997. To understand the observational data and to estimate the abundances it is necessary to adopt for the nebula at least a two-component structure consisting of a more dense inner zone enclosed in a shell of lower density.

Our aim was to determine the physical conditions in the nebula, so we measured several diagnostic ratios. The most actively used intensity ratio has always been the relation involving the auroral [OIII] $\lambda 4363$ and one or both of the nebular [OIII] $\lambda 4959, 5007$ transitions. We did not always manage to measure the $\lambda 5007$ line intensity, therefore Figure 8 shows the change of the $R = F(\lambda 4363)/F(\lambda 4959)$ value over a time period of about 80 years. In 2010–2019 the ratio decreased thus keeping the tendency started about 1990, and by 2019 it returned to the value observed in 1960–1970. Due to the availability of absolute intensities, we can schematically divide the evolution of R in 1970–2019 into three intervals. During the first phase (~ 1970 –1990) R was growing due to the strengthening of the auroral transition and weakening of the nebular one; at the second stage (~ 1990 –2000) – R was decreasing with the simultaneous strengthening of both lines; during the third phase (~ 2000 –2019) – R was decreasing due to the strengthening of the nebular transition and weakening of the auroral one. The big grey circles in Figures 6 и 8 indicate the averaged values of corresponding quantities at the points which delimit the highlighted intervals: 1970, 1990, 2003 (the year when we started our spectroscopic monitoring with a CCD), 2019.

Some other line ratios seem to be variable too, though their variation can be traced over a shorter period of time and is not evident (see Figure 9). So, the [ArIII] $F(\lambda 5192)/F(\lambda 7135)$ ratio was observed to decrease from ~ 0.033 in the early 1990s (Hyung et al., 1994) to ≤ 0.01 (this work) in 2019. The [ArIII] $\lambda 5192$ line, however, is very weak and forms a blend with two other lines of comparable intensity, [NI] $\lambda 5198$ и $\lambda 5200$, and the low dispersion makes its measuring uncertain. Similar behavior is seen for the [SIII] lines, though a large wavelength separation between them ($\lambda 6312$ and $\lambda 9069$) leads to a significant calibration uncertainty. On the contrary, the [NII] $F(\lambda 5755)/F(\lambda 6584)$ ratio does not show any significant change. Besides, the scatter of estimates is big, possibly due to the difficulty in separating the $\lambda 6584$ line from the $H\alpha$ wing.

The diagnostic relations sensitive to electron density, [SII] $F(\lambda 6716)/F(\lambda 6731)$ and [ClIII] $F(\lambda 5518)/F(\lambda 5538)$, stayed constant within the limits of accuracy over the whole period of our observations since 2003. The $F(\lambda 6716)/F(\lambda 6731)$ ratio is close to its critical value, so it indicates only the lower limit of $\log N_e \sim 4$ which corresponds to the outer envelope of lower density where the low excitation species emit. The ratio of [ClIII] lines is also close to its critical value. This ratio is attributed to the zones of higher excitation and suggests a somewhat higher estimate for the density of $\lg N_e \sim 4.5$. But the second ionization potential for chlorine is lower than that for oxygen, therefore the zone where the $\lambda 5518, 5538$ lines originate may match only partially with the [OIII] emitting region. The constancy of the ratios mentioned above implies that even if the electron density in the low excitation zones varies it does not fall much lower than the critical value ($\lg N_e^{crit} \sim 3 - 3.5$ for sulphur и $\sim 4 - 4.5$ for chlorine).

Let's now consider the displacement of diagnostic curves representing the ions N^+ , S^{2+} , O^{2+} and Ar^{2+} in the $N_e - T_e$ diagram. These ions have a similar structure of energetic levels but differ in the ionization potential and critical density, and must emit in different regions of the nebula. Figure 10 contains the $N_e - T_e$ diagrams constructed by means of the PyNeb package (Luridiana et al., 2015) for the moments which limit the intervals of time highlighted according to the change of the [OIII] absolute intensities. Besides the fact that one pair of N_e, T_e values can not explain the observed data, the total appearance of the diagrams suggests a high value of the electron density ($\lg N_e \geq 6$), at least for the strata where the [OIII] lines arise. The ratios used for the diagrams were corrected for the interstellar reddening with $c(H\beta) = 0.35$. The diagram for the year 1990 was drawn basing on the data from Hyung et al. (1994), and they derived $c(H\beta) = 0.8$. If we had corrected the ratios using this value of $c(H\beta)$, the diagnostic curves would have been located in the area of larger values of N_e, T_e . Since 1990 the curves associated with O^{2+} , S^{2+} и Ar^{2+} evolved in similar manner, they shifted to the smaller values of N_e, T_e , while the location of the N^+ curve almost did not change. Probably, the variation of N_e, T_e does not affect the [NII] emitting zone.

As we are not able to derive the absolute N_e, T_e values for the given epochs, let's try to determine how they change. The initial data for our further calculations are the changes of absolute intensities for $H\beta$, [OIII] $\lambda 4363, 4959$, and also the changes of their relations corrected for reddening. We assume that the zones where all these transitions arise are characterized by the same N_e, T_e values and the number of emitting hydrogen atoms is constant. Some definite value of temperature is considered as an initial one (in 1970). First, we find N_e for this initial moment using R , and the relative abundance of O^{2+} using relative intensities. Then, as we know the relative change of $F(H\beta)$ between the two epochs and the R value at the second moment, we can estimate N_e, T_e at the second moment and also the abundance of O^{2+} using relative intensities. The same procedure is executed as we pass from the second moment to the third and from the third to the fourth. Table 6 lists the results of the simulations performed by means of the package PyNeb for several initial values of the electron temperature: $T_e = 8000, 10000, 12000$ K. For all initial temperatures, N_e varies only slightly, whereas T_e first grows and then drops by several thousand degrees.

A significant growth of temperature is necessary to interpret the decrease in the absolute intensity of $H\beta$ since 1970. It could have been explained by the decrease in N_e , but it is in contrary to the growth of R . On the other hand, the intensity of collision excited lines must increase with temperature, but we observe the nebular lines decreasing since 1970, and the auroral line increasing is less than expected for such change in temperature. To explain the observed data it's necessary to reduce significantly the number of emitting O^{2+} ions (by a factor of 10), which may be due to the subsequent ionization of oxygen or to the diminution of the emitting zone.

And the question arises: what did make T_e to increase by several thousand degrees? According to Ferland (1979), if the change in the electron temperature of the nebula is caused by a change in the flux of ionizing photons Q from the central star, we can relate them through an equation: $\Delta T_e \simeq 4200 \times \Delta Q / Q$. So, the 300 K temperature change proposed by Ferland to explain fast variability of the $F(\lambda 4363) / F(H\gamma)$ ratio requires an 8% change in the ionizing flux. But our simulations imply a temperature increase of several thousand degrees that would mean ionizing flux increasing by several times. We find it hard to imagine such a process. A rise in T_e must have been caused not so much by the growth in the effective temperature of the star because the level of excitation of the spectrum of IC 4997 did not change over the observed period, but by some other processes, for instance, the interaction of stellar winds.

Table 6 also lists the relative intensities for the HeI $\lambda 5876$ line calculated using the obtained values of N_e, T_e and $He^+ / H^+ = 0.1$. One can see that in the case of the initial $T_e = 8000$ K the intensity changes only slightly, whereas for $T_e \geq 10000$ K the simulated variation of intensity matches qualitatively with the observed one, though the amplitude is smaller.

The results presented in Table 6 can be considered as a kind of estimation. A larger value of interstellar reddening ($c(H\beta) > 0.35$) will require a larger increase in electron temperature to explain the observed spectral changes. If we take into account the fact that we measure the integral flux from the nebula, whereas the fluctuation of N_e, T_e may occur only in some strata, then the amplitude of temperature change will be larger.

DISCUSSION AND CONCLUSIONS

We have presented optical and near IR photometric and low-resolution spectroscopic data for IC 4997 obtained in 2009–2019. New results are investigated together with the previously published data.

Basing on the observational data obtained with our invariable UBV photometric system we have plotted an annual average light curve of IC 4997 from 1970 till 2019. We have found a long-term marked dip in UBV flux with a peak-to-peak range of 0.5^m in V . The source started fading after 1970, reached the minimum brightness near 1985, then recovered to the initial level in B and U , whereas

the V brightness continued growing up to 2019. In 2019 we obtained new near IR $JHKL$ photometric data. The nebula was found to be fainter in 2019 if compared to the epoch of 1999–2006 with the effect most prominent in L . We have shown that the long-term optical and IR brightness variation is related mostly to the changing input from the nebular emission lines.

After the emission contribution was subtracted from the B and V brightness, the $B - V$ color of the integral continuum corrected for reddening appeared still too red for a sum of the stellar and gas continua, which may be indicative of the presence of one more source of continuum radiation in this wavelength range (a satellite of the central star?), although the evidence is very uncertain. It's worth mentioning that the central star of IC 4997 is not only suspected to be binary but it was also included in the list of PN possibly shaped by a triple stellar system (= *maybe triple* class) with a probability of 0.33.

Basing on new and previously published data we have traced the evolution of relative and absolute intensities and their relations for some emission lines originated in the nebula over a period 1970–2019. In 2010–2018 the $\lambda 4363/H\gamma$ ratio decreased as it had been doing since about 1990 and by 2019 returned to the value observed in 1960–1970. Over the whole period of observations the ratio drew a wave with a peak-to-peak amplitude of 0.45 in logarithmic scale and a characteristic time of 50-60 years.

With the use of archival and new data we have traced the evolution of absolute intensity for $H\beta$: one can note a period of higher values before 1980, a fading by a factor of 1.5 and subsequent maintenance at the same level with a slight tendency to growth till 2000–2005, then a more pronounced increase. The variation of the absolute intensity of the nebular [OIII] $\lambda 4959$ line in 1960-2019 was roughly similar to that of $H\beta$ but had a larger amplitude ($F_{max}/F_{min} \geq 2$). Having recovered to the value observed before fading, the absolute intensity of [OIII] $\lambda 4959$ did not change significantly in 2010-2019. The absolute intensity of the auroral [OIII] $\lambda 4363$ line grew since 1960 at a nearly constant rate, reached maximum value about 2000-2005 having increased more than twice, then started to fade and is still fading.

We have also reconstructed the variations of intensity for some other transitions. In particular, we have traced the variability of HeI $\lambda 5876$ in 1960-2019: an increase in relative intensity by a factor of ~ 2 , then weakening and return to the former level.

We have estimated the lower limit for the electron density in the outer shell of IC 4997 using the diagnostic ratios of [SII] η [ClIII]: $\lg N_e \sim 4$ $\eta \sim 4.5$ respectively. The ratios stayed constant within errors and were close to critical values in 2010-2019.

The location of diagnostic curves of N^+ , S^{2+} , O^{2+} and Ar^{2+} on the N_e, T_e plane indicates that, first, there are zones of different electron temperature and density in the nebula, and, second, the parameters vary with time. A rise in one or both of these characteristics was observed at least in the inner part of the nebula in 1970-1990 with subsequent decrease which lasts until now. Using the data on absolute intensity variations for $H\beta$, [OIII] $\lambda 4363, 4959$ and assuming that N_e, T_e are the same for the strata where these lines arise, we have estimated the scale of the variation. We think that the variation of T_e in the inner part of the nebula is responsible for the spectral variability of IC 4997, and the change in T_e is due not so much to the change in ionizing flux from the central star, but to the variable stellar wind and the related processes. In general, the spectral changes observed in 1960-2019 may be interpreted as the observable consequence of a single episode of enhanced mass loss from the variable central star. There are still the questions of what has triggered the increase in mass loss rate, whether this episode was a unique one or could occur again in one form or another.

ACKNOWLEDGEMENT

The authors dedicate this paper to the memory of Doctor of Science Elena B. Kostyakova, Senior Researcher Fellow at the Sternberg Astronomical Institute (1924–2013).

This research has made use of the ADS, SIMBAD and VIZIER databases.

REFERENCES

1. A. Acker, J. Koppen, B. Stenholm, and G. Jasiewicz, *Astron. Astrophys. Suppl. Ser.* **80**, 201 (1989)
2. A. Acker, J. Marcout, F. Ochsenbein, et al., *The Strasbourg-ESO Catalogue of Galactic Planetary Nebulae, Parts I, II*, (1992)
3. F.A. Ahern, *Astrophys. J.* **223**, 901 (1978)
4. L.H. Aller, *Astrophys. J.* **93**, 236 (1941)
5. L.H. Aller and J.B. Kaler, *Astrophys. J.* **140**, 621 (1964)
6. L.H. Aller and W. Liller, *MNRAS* **132**, 337 (1966)
7. L.H. Aller and M.F. Walker, *Astrophys. J.* **161**, 917 (1970).
8. V.P. Arkhipova, E.B. Kostyakova, R.I. Noskova, *Astron. Lett.* **20**, 99 (1994)
9. E. Bear, N. Soker, *MNRAS* **837**, L10 (2017)
10. M.A. Burlak, V.F. Esipov, *Astron. Lett.*, **36**, 752 (2010)
11. S. Casassus, L.-Å. Nyman, C. Dickinson, and T. J. Pearson, *MNRAS* **382**, 1607 (2007)
12. W.A. Feibelman, R.W. Hobbs, C.W. Mc Cracken, L.W. Brown, *Astrophys. J.* **231**, 111 (1979)
13. G.J. Ferland, *MNRAS* **188**, 669 (1979)
14. F.C. Gillett, R.F. Knacke, W.A. Stein, *Astrophys. J.* **163**, L57-59, 1971
15. I.N. Glushneva, V.T. Doroshenko, T.S. Fetisova, T.S. Khruzina, E.A. Kolotilov, L.V. Mossakovskaya, S.L. Ovchinnikov, and I.B. Voloshina, *VizieR Online Data Catalog III/208* (1998).
16. Y. Gómez, L.F. Miranda, J.M. Torrelles, L.F. Rodríguez, J.A. López, *MNRAS* **336**, 1139 (2002)
17. G.A. Gurzadian G.A., *Soviet Astronomy* **2**, 482 (1958)
18. M.Hajduk, P.A.M. van Hoof, and A.A. Zijlstra, *Astron. and Astrophys.***J.573** , A65 (2015)
19. W.A. Hiltner, B. Iriarte, M.L. Johnson, *Astrophys. J.* **127**, 539 (1958)
20. S. Hyung, L.H. Aller, *Proc. Nat. Acad. Sci. USA* **90**, 413 (1993)
21. S. Hyung, L.H. Aller, W.A. Feibelman, *Astrophys. J. Suppl. Ser.* **93**, 465 (1994)
22. H.L. Johnson, R.I. Mitchel, B. Iriarte, W.Z. Wisniewski, *Comm. Lunar and Planet. Lab.* **4**, 99 (1966).
23. G.S. Khromov, *Sov. Astron.* **5**, 619 (1962)
24. E.B. Kostyakova, *Sov. Astron.* **14**, 794 (1971)

25. E.B. Kostyakova, *Astron. Lett.* **16**, 465 (1990)
26. E.B. Kostyakova, *Trudy GAISH*, **62**, 143, (1991)
27. E.B. Kostyakova, *Astron. Lett.* **25**, 389 (1999)
28. E.B. Kostyakova, V.P. Arkhipova, *Astron. Rep.* **53**, 1155 (2009)
29. E.B. Kostyakova, V.P. Arkhipova, M.V. Savel'eva, *Mem. Soc. Roy. Sci. Liege, 6 Ser.*, **5**, 473 (1973)
30. P. Lenzuni, A. Natta, N. Panagia, *Astrophys. J.* **345**, 306 (1989)
31. W. Liller and L.H. Aller, *Sky and Tel.* **16**, 222 (1957)
32. W. Liller and L.H. Aller, *Proc. Nat. Acad. Sci.* **49**, 695 (1963)
33. V. Luridiana, C. Morisset, and R.A. Shaw, *Astron. Astrophys.* **573**, 42 (2015)
34. V. M. Lyutyi, *Soobshch. GAISH* **172**, 30 (1971)
35. W.L.F. Marcolino, and F.X. de Araújo, *Astron. J.* **126**, 887 (2003)
36. W.L.F. Marcolino, F.X. de Araújo, H.B.M. Junior, and E.S. Duarte, *Astron. J.*, **134**, 1380 (2007)
37. D.H. Menzel, L.H. Aller, M.H. Hebb, *Astrophys. J.* **93**, 230 (1941)
38. L.F. Miranda, J.M. Torrelles, C. Eiroa, *Astrophys. J.* **461**, L111 (1996)
39. L.F. Miranda, J.M. Torrelles, *Astrophys. J.* **496**, 274 (1998)
40. A. Natta, N. Panagia, *Astrophys. J.* **248**, 185 (1981)
41. C.R. O'Dell, *Astrophys. J.* **138**, 1018 (1963)
42. R. Ohsawa, T. Onaka, I. Sakon, M. Matsuura, H. Kaneda, *Astron. J.* **151**, 93 (2016)
43. T.L. Page, *Astrophys. J.* **96**, 78 (1942)
44. Q.A. Parker, I.S. Bojičić, D.J. Frew, *Journal of Physics: Conference Series* **728**, article id. 032008 (2016)
45. B.M. Pazderska, M.P. Gawroński, R. Feiler, M. Birkinshaw, I.W.A. Browne, R. Davis, A.J. Kus, K. Lancaster, S.R. Lowe, E. Pazderski, M. Peel and P.N. Wilkinson, *Astron. Astrophys.* **498**, 463 (2009)
46. A.J. Pickles, *Publ. Astron. Soc. Pacific* **110**, 863 (1998).
47. S.R. Pottasch, B. Baud, D. Beinteme, J. Emerson et al., *Astron. Astrophys.* **138**, 10 (1984)
48. A.T. Purgathofer, *Circ. IAU* **3258** (1978)
49. A.T. Purgathofer and M. Stoll, *Astron. Astrophys.* **99**, 218 (1981)
50. R. Sahai, M.R. Morris, and G. Villar, *Astron. J.* **141**, 134 (2011)
51. O. Struve and P. Swings, *Astrophys. J.* **93**, 356 (1941)

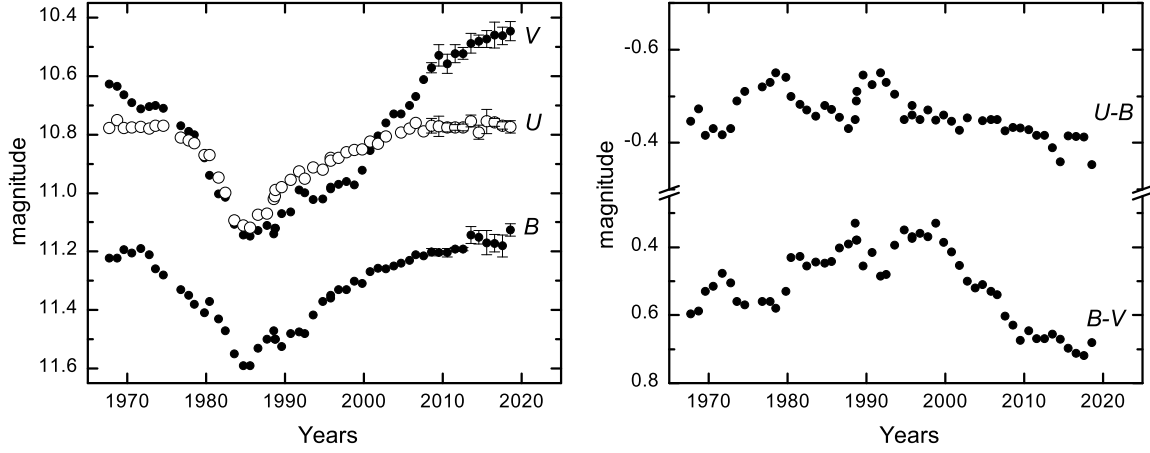


Figure 1: The annual average UBV light and $U - B, B - V$ color curves for IC 4997 in 1968–2019.

52. O.G. Taranova, V.I. Shenavrin, *Astron. Lett.* **33**, 584 (2007)
53. B.A. Vorontsov-Velyaminov, *Sov. Astron.* **4**, 929 (1960)
54. B.A. Vorontsov-Velyaminov, E.B. Kostyakova, O.D. Dokuchaeva, V.P. Arkhipova, *Sov. Astron.* **9**, 364 (1965)
55. B.A. Vorontsov-Velyaminov, E.B. Kostyakova, O.D. Dokuchaeva, V.P. Arkhipova, *Trudy GAISH* **40**, 57 (1970)
56. M.L. White, *Astrophys. J.* **115**, 71 (1952)
57. P.A. Whitelock, *MNRAS* **213**, 59 (1985)

Table 1: UBV photometry for IC 4997 in 2009–2019.

JD	V	B	U
2455031	10.552	11.200	10.770
2455038	10.549	11.213	10.768
2455042	10.578	11.204	10.786
2455057	10.575	11.197	10.810
2455061	10.579	11.210	10.761
2455068	10.561	11.214	10.771
2455086	10.572	11.183	10.716
2455092	10.582	11.186	10.763
2455095	10.604	11.212	10.775

Table 1 –

JD	<i>V</i>	<i>B</i>	<i>U</i>
2455331	10.601	11.214	10.719
2455362	10.543	11.204	10.784
2455363	10.529	11.192	10.772
2455399	10.528	11.207	10.830
2455410	10.495	11.200	10.744
2455413	10.489	11.202	10.769
2455422	10.519	11.205	10.787
2455662	10.543	11.204	10.784
2455663	10.529	11.192	10.772
2455737	10.544	11.194	10.772
2455743	10.565	11.200	10.784
2455750	10.569	11.192	10.766
2455754	10.531	11.190	10.792
2455766	10.535	11.209	10.765
2455774	10.529	11.206	10.767
2455779	10.554	11.204	10.767
2455780	10.650	11.248	10.811
2455782	10.542	11.188	10.771
2455794	10.552	11.205	10.777
2455861	10.570	11.211	10.750
2455866	10.598	11.215	10.782
2456101	10.515	11.196	10.767
2456121	10.484	11.184	10.791
2456122	10.531	11.186	10.780
2456123	10.511	11.187	10.779
2456130	10.483	11.191	10.776
2456153	10.561	11.198	10.783
2456155	10.563	11.198	10.774
2456161	10.534	11.200	10.757
2456448	10.520	11.188	10.760
2456457	10.514	11.188	10.789
2456464	10.505	11.189	10.779
2456483	10.522	11.190	10.772
2456504	10.518	11.188	10.764
2456514	10.495	11.183	10.775
2456518	10.503	11.188	10.797
2456575	10.552	11.202	10.778
2456605	10.553	11.199	10.780
2456607	10.540	11.200	10.765
2456839	10.486	11.131	10.765
2456868	10.477	11.132	10.765
2456875	10.468	11.108	10.744
2456885	10.442	11.147	10.715
2456893	10.506	11.123	10.775

Table 1 –

JD	<i>V</i>	<i>B</i>	<i>U</i>
2456944	10.547	11.170	10.746
2457213	10.484	11.130	10.827
2457216	10.478	11.138	10.778
2457220	10.497	11.136	10.778
2457253	10.501	11.183	10.810
2457270	10.447	11.169	10.767
2457550	10.487	11.200	10.774
2457578	10.506	11.128	10.768
2457583	10.457	11.142	10.784
2457640	10.442	11.210	10.694
2457935	10.442	11.196	10.742
2457950	10.478	11.195	10.749
2457958	10.487	11.189	10.740
2457959	10.481	11.166	10.781
2457967	10.440	11.199	10.751
2457969	10.386	11.190	10.750
2457979	10.416	11.124	10.766
2457986	10.448	11.131	10.775
2457994	10.461	11.126	10.766
2458013	10.454	11.182	10.763
2458046	10.564	11.192	10.761
2458282	10.449	11.187	10.754
2458306	10.499	11.193	10.786
2458347	10.418	11.182	10.770
2458364	10.471	11.121	10.773
2458435	10.474	11.220	10.760
2458613	10.490	11.191	10.773
2458636	10.425	11.141	10.789
2458638	10.434	11.119	10.785
2458647	10.445	11.123	10.756
2458658	10.437	11.120	10.781
2458661	10.449	11.130	10.776
2458677	10.443	11.132	10.758
2458691	10.440	11.111	10.743
2458701	10.468	11.118	10.778
2458704	10.441	11.124	10.768
2458719	10.388	11.103	10.794
2458720	10.415	11.119	10.727
2458721	10.399	11.112	10.743
2458725	10.446	11.126	10.804
2458733	10.472	11.101	10.761
2458752	10.477	11.119	10.774
2458760	10.485	11.107	10.797
2458778	10.472	11.127	10.795

Table 1 –

JD	<i>V</i>	<i>B</i>	<i>U</i>
2458789	10.492	11.129	10.787

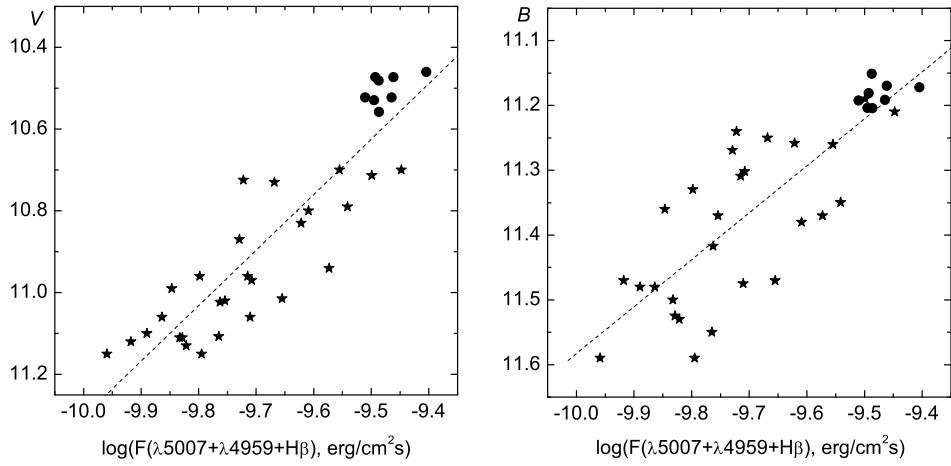


Figure 2: The relationship between $\lg(F(H\beta) + F(\lambda 4959) + F(\lambda 5007))$ and the V and B brightness in 1972–2019. The asterisks represent the data from Kostyakova and Arkhipova (2009), the points – this work.

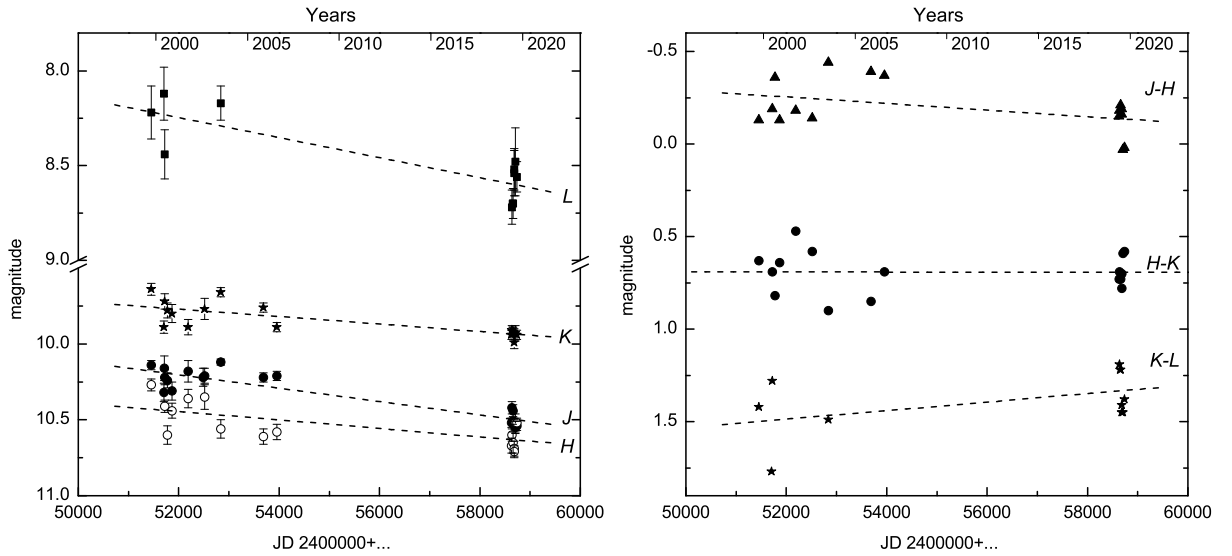


Figure 3: The change in near IR brightness and color for IC 4997 in 1999–2019.

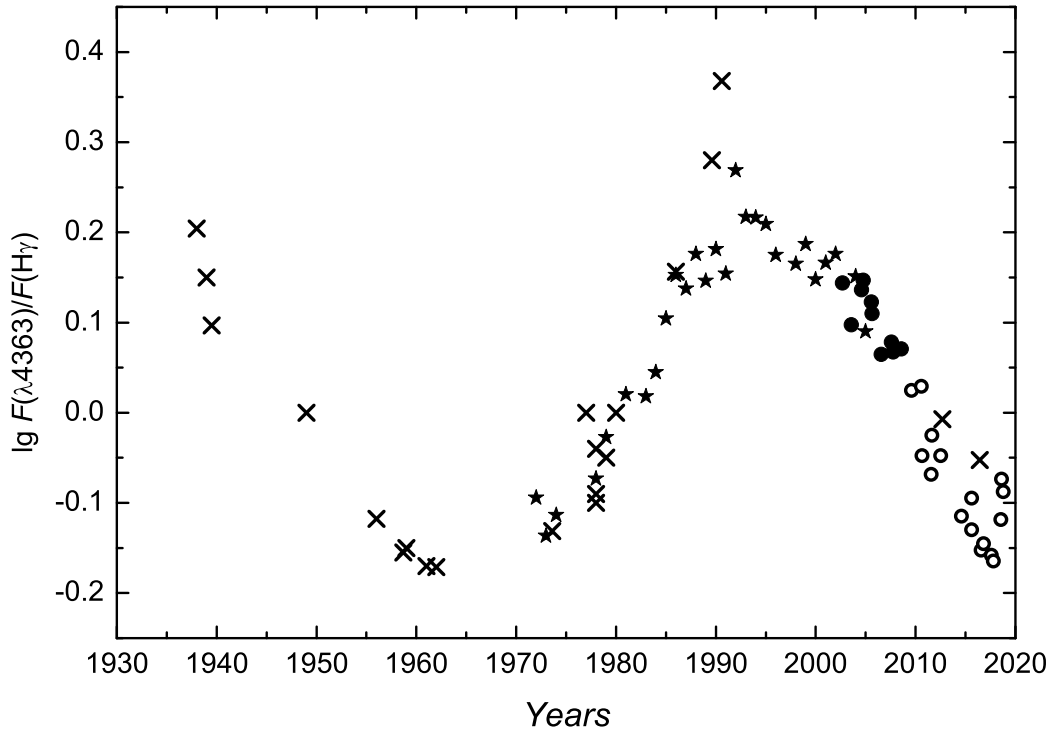


Figure 4: The evolution of the observed intensity ratio $F(\lambda 4363)/F(H\gamma)$ based on data from different studies: asterisks – Kostyakova, Arkhipova (2009), filled circles – Burlak, Esipov (2010), open circles – this work, crosses – other sources, see the references in the text.

Table 2: The annual average UBV magnitudes for IC 4997 in 2009-2019.

Year	V	σ_V	B	σ_B	U	σ_U	N
2008.6	10.572	0.017	11.202	0.012	10.769	0.012	10
2009.5	10.529	0.037	11.204	0.007	10.772	0.035	7
2011.6	10.523	0.031	11.192	0.006	10.776	0.010	8
2010.6	10.558	0.035	11.204	0.015	10.776	0.015	14
2012.6	10.523	0.020	11.191	0.006	10.776	0.011	10
2013.6	10.488	0.033	11.135	0.021	10.754	0.020	7
2014.6	10.481	0.021	11.151	0.023	10.792	0.025	5
2015.6	10.473	0.029	11.170	0.041	10.755	0.041	4
2016.6	10.460	0.045	11.172	0.030	10.759	0.013	11
2017.6	10.462	0.030	11.180	0.037	10.769	0.012	5
2018.6	10.447	0.033	11.127	0.021	10.774	0.021	19

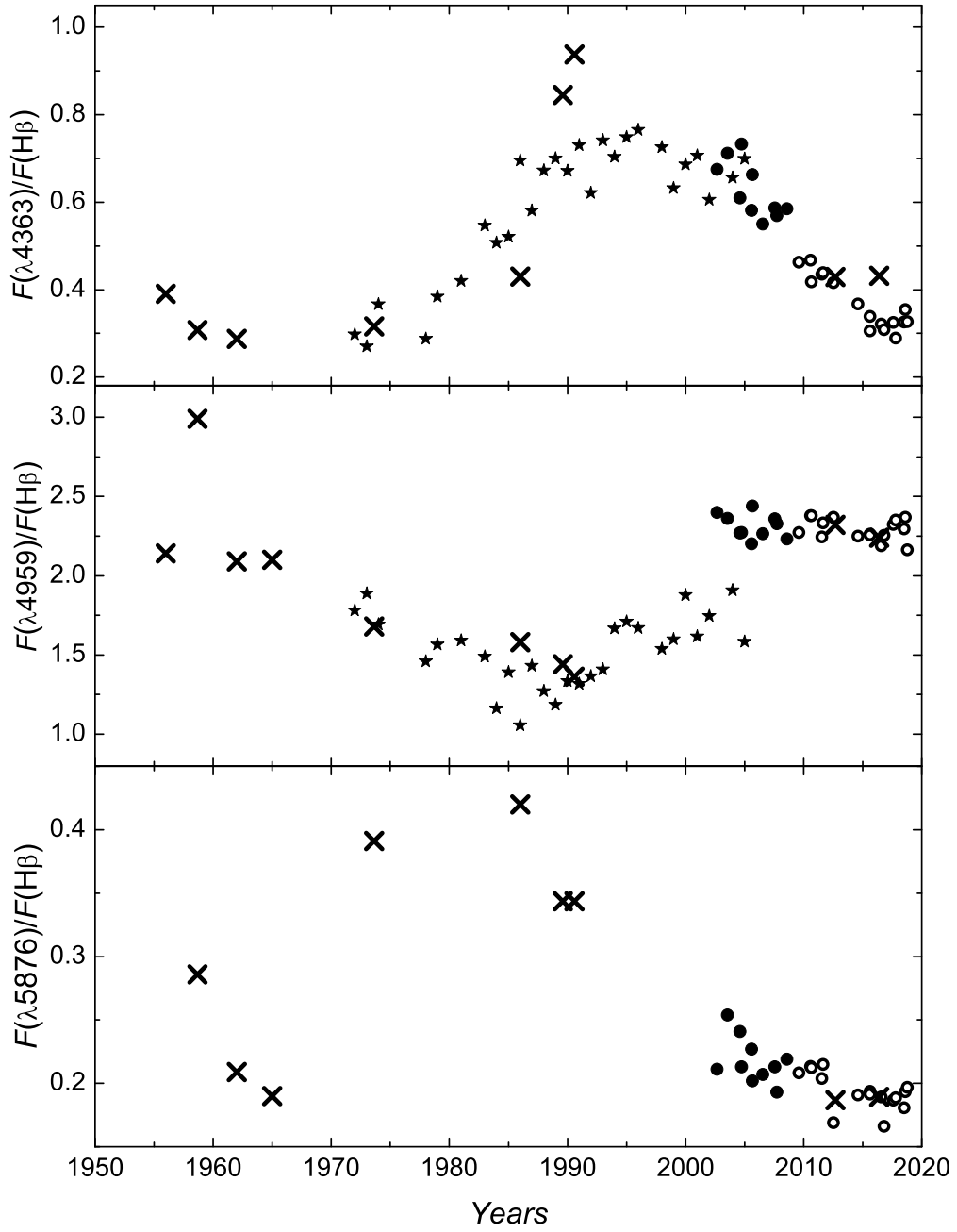


Figure 5: The evolution of the observed relative intensities of [OIII] λ 4363, λ 4959 and HeI λ 5876 based on data from various sources. The symbols are the same as for Figure 4.

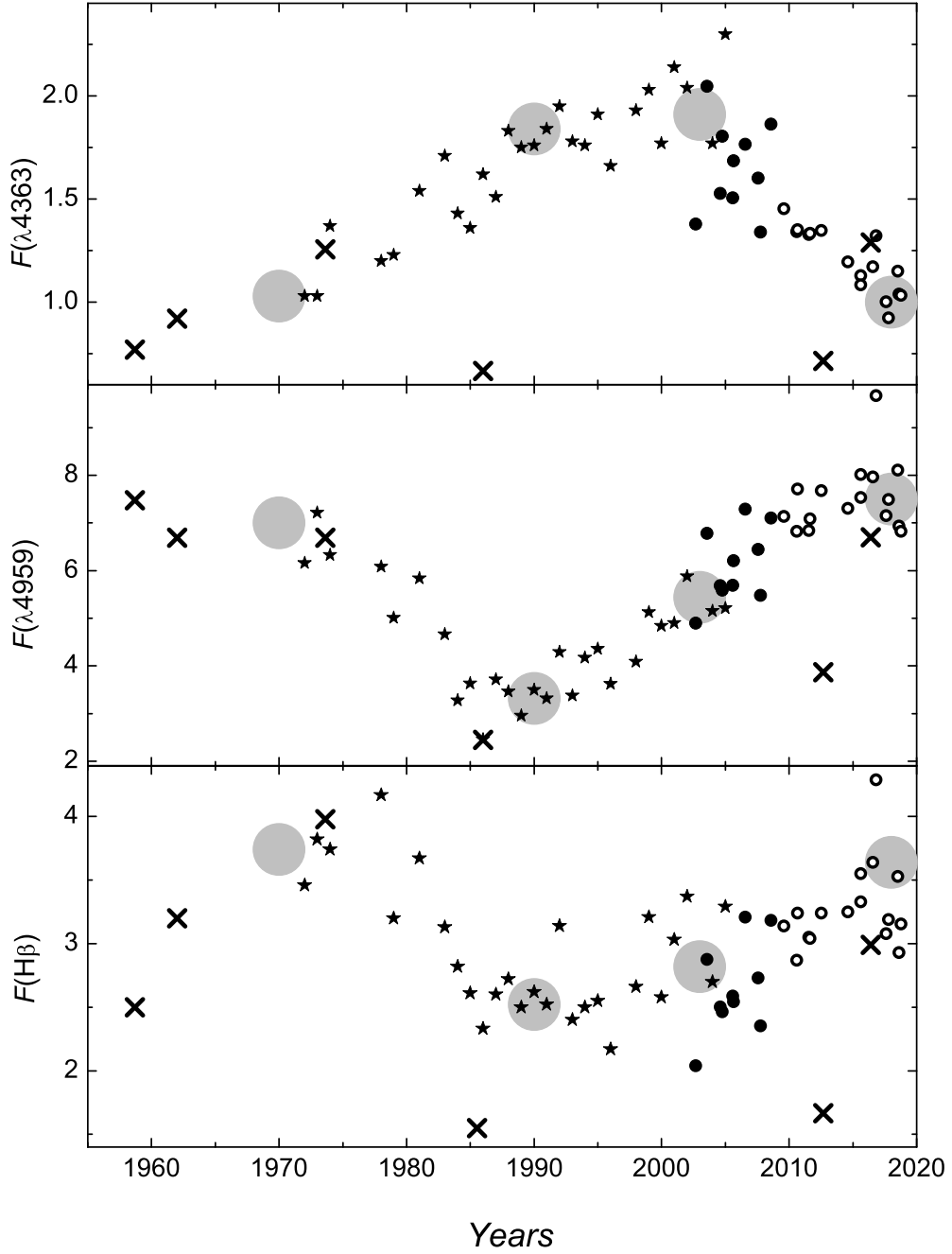


Figure 6: The evolution of the observed absolute intensities of [OIII] $\lambda 4363$, $\lambda 4959$ and $H\beta$ expressed in units of $10^{-11} \text{ erg cm}^{-2}\text{s}^{-1}$. The symbols are the same as for Figure 4. Big grey circles represent average values at the points that delimit the time intervals distinguished by the peculiarities of [OIII] $\lambda 4363$ and $\lambda 4959$ variations.

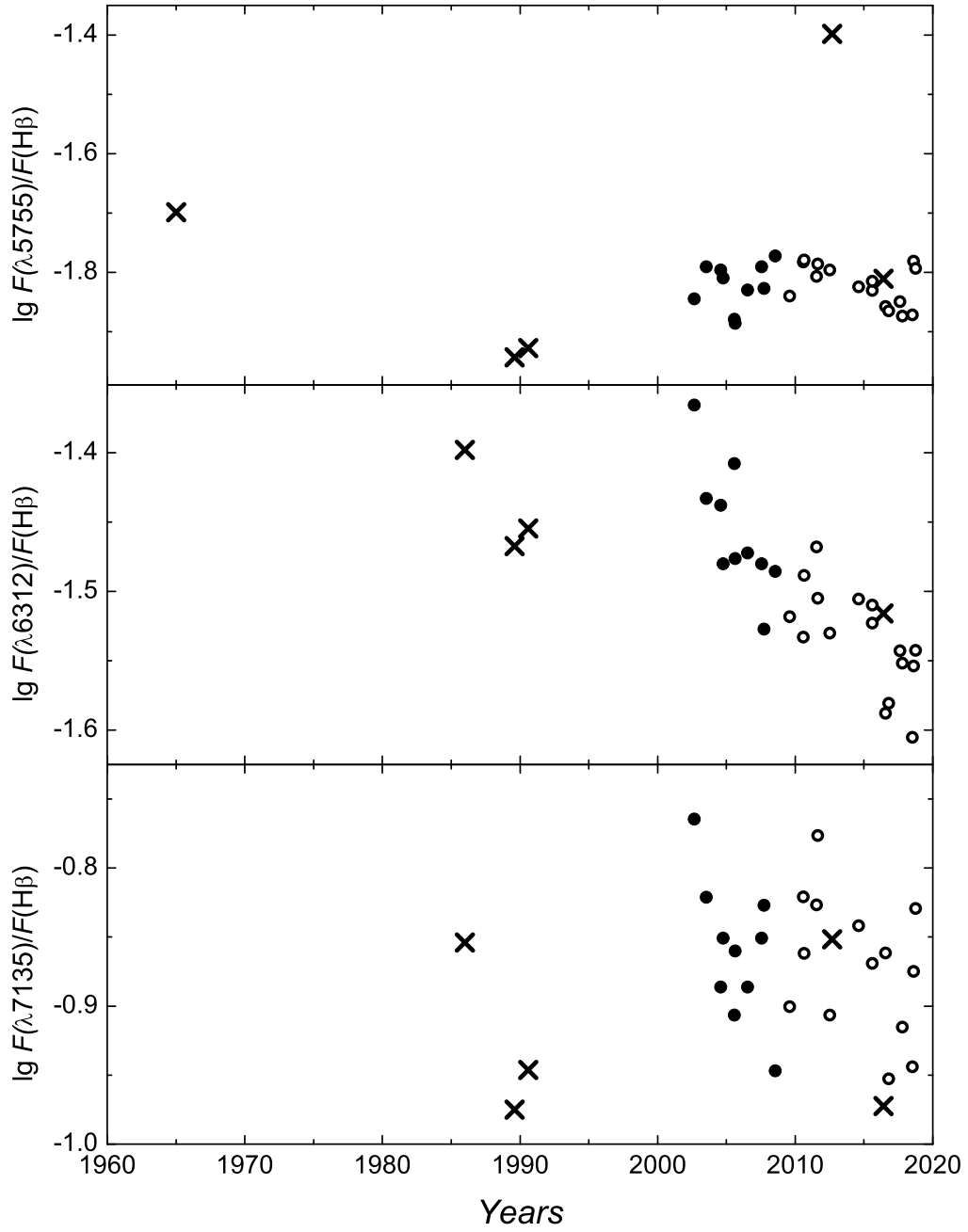


Figure 7: The evolution of the observed relative intensities of [ArIII] $\lambda 7135$, [SIII] $\lambda 6312$, [NII] $\lambda 5755$ based on data from various sources. The symbols are the same as for Figure 4.

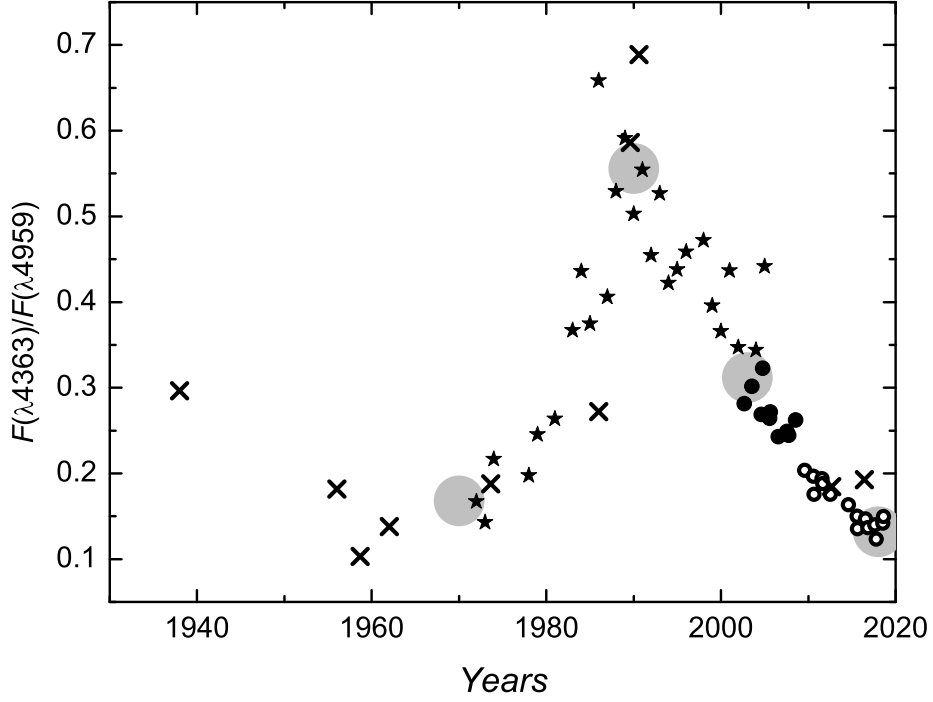


Figure 8: The evolution of the observed auroral to nebular line ratio $F(\lambda 4363)/F(\lambda 4959)$ based on data from various sources. The symbols are the same as for Figures 4 and 6.

Table 3: $JHKL$ photometry for IC 4997 in 2019.

JD	J	σ_J	H	σ_H	K	σ_K	L	σ_L
2458631.5	10.52	0.03	10.67	0.05	9.94	0.03	–	–
2458634.5	10.42	0.04	10.60	0.04	9.91	0.03	8.72	0.09
2458631.5	10.52	0.03	10.67	0.05	9.94	0.03	–	–
2458655.5	10.51	0.02	–	–	9.92	0.03	8.70	–
2458659.5	10.44	0.04	10.65	0.07	9.92	0.03	8.70	0.08
2458682.5	10.53	0.03	10.69	0.05	9.99	0.04	8.54	0.12
2458686.5	10.52	0.03	10.71	0.04	9.93	0.03	8.52	0.11
2458704.5	10.55	0.04	10.52	0.06	9.93	0.05	8.48	0.18
2458734.3	10.54	0.03	10.52	0.03	9.94	0.03	8.56	0.08
2458776.2	10.47	0.03	10.64	0.03	9.95	0.02	8.61	0.10

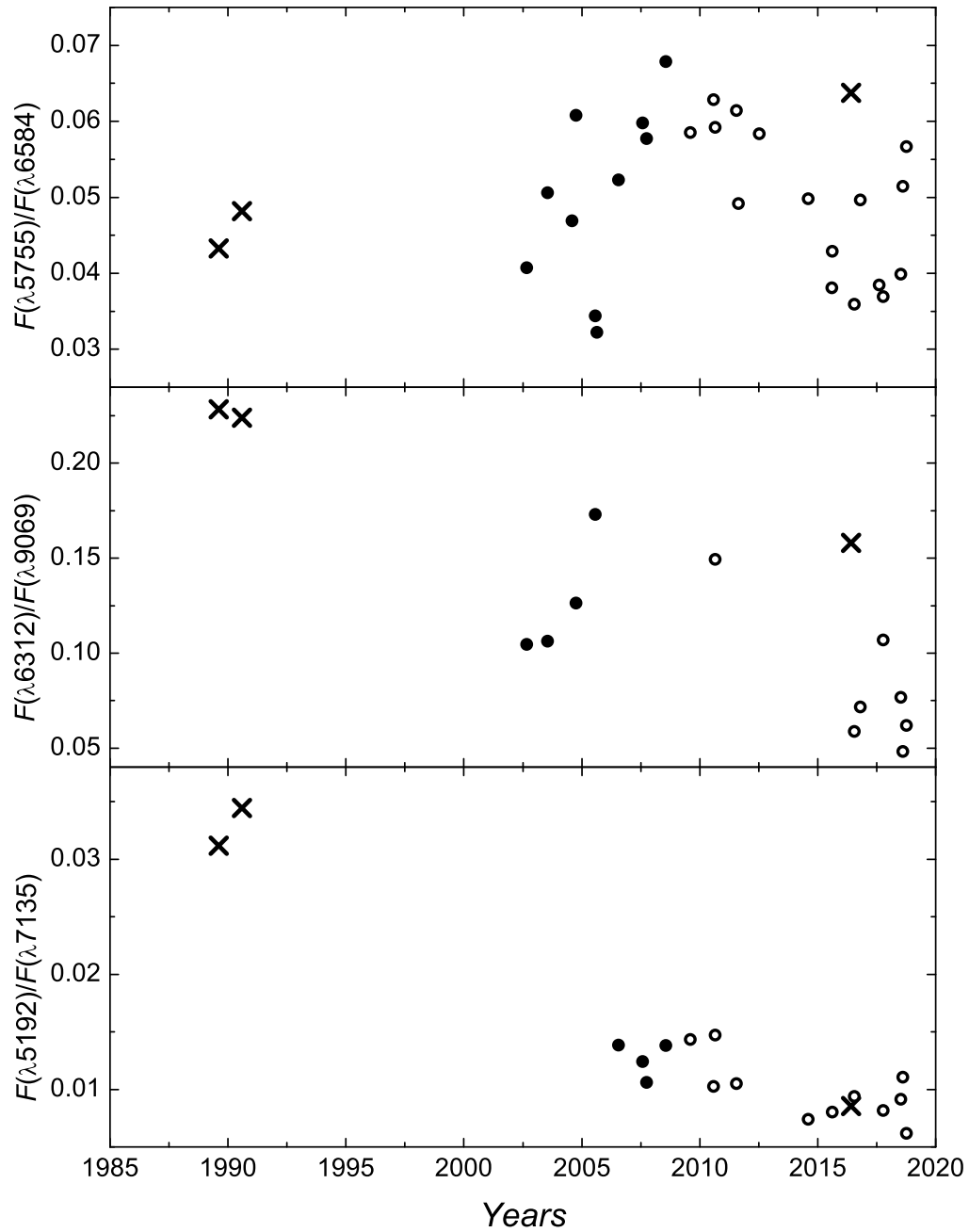


Figure 9: The evolution of the observed auroral to nebular line ratios [ArIII] $F(\lambda 5192)/F(\lambda 7135)$, [SIII] $F(\lambda 6312)/F(\lambda 9069)$, [NII] $F(\lambda 5755)/F(\lambda 6584)$ based on data from various sources. The symbols are the same as for Figure 4.

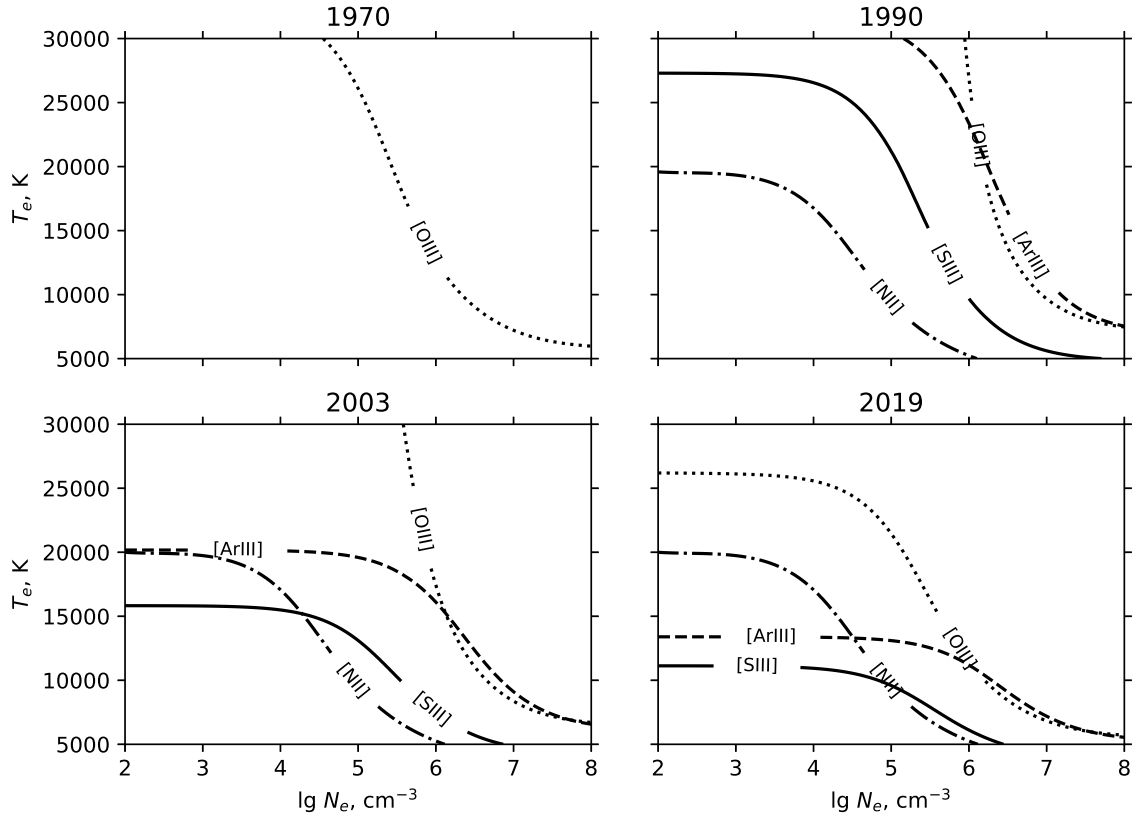


Figure 10: Diagnostic diagrams for IC 4997 drawn with the use of averaged data from different sources for the epochs of 1970, 1990, 2003 and 2019. All the intensity ratios were corrected for interstellar reddening with $c(H\beta) = 0.35$. Different lines indicate ions: solid for [SIII], dotted for [OIII], dashed for [ArIII], and dotted-dashed for [NII].

Table 4: Log of spectroscopic observations of IC 4997.

Date	JD	Range, Å	Standard
04.08.2010	2455413	4000–7200	18 Vul
31.07.2011	2455774	4000–7400	HD 196775
26.08.2011	2455800	4000–9100	40 Cyg
21.07.2012	2456130	4000–7400	18 Vul
23.08.2012	2456163	4200–7400	ρ Aql
09.07.2013	2456483	4000–7200	29 Vul
08.08.2015	2457243	4000–7700	107 Her
06.08.2016	2457607	4000–6700	ρ Aql
09.08.2016	2457610	4000–7700	ρ Aql
21.07.2017	2457956	4000–9700	ρ Aql
19.10.2017	2458046	4000–9700	ρ Aql
08.08.2018	2458339	4000–7000	29 Vul
13.10.2018	2458405	4000–9400	29 Vul
07.07.2019	2458672	4000–9400	29 Vul, 30 Vul
07.08.2019	2458703	4000–9250	29 Vul, HD 196775, η Sge
03.10.2019	2458760	4000–9250	HD 196775, η Sge

Table 5: The observed relative intensities of emission lines for IC 4997 on the scale $I(\text{H}\beta) = 100$ and the observed intensity of $\text{H}\beta$ in units of $10^{-11} \text{ erg cm}^{-2}\text{s}^{-1}$.

λ , Å	Ion	04.08.10	31.07.11	26.08.11	21.07.12	23.08.12	09.07.13	08.08.15	06.08.16
4102	H δ	20.1	20.7	20.9	23.8	-	21.6	21.9	21.4
4340	H γ	43.7	43.7	46.6	51.0	46.5	46.4	47.9	42.2
4363	[OIII]	46.3	46.8	41.8	43.5	43.9	41.6	36.8	33.9
4471	HeI	4.01	4.35	4.47	4.81	4.13	4.54	4.45	4.16
4713	HeI	0.94	0.97	0.85	0.97	-	0.97	0.81	0.76
4740	[ArIV]	0.38	0.45	0.41	0.43	-	0.42	0.37	0.34
4959	[OIII]	227	238	238	224	233	237	225	226
5007	[OIII]	690	725	734	680	691	723	678	-
5192	[ArIII]	0.18	0.16	0.20	0.16	-	-	0.11	0.11
5270	[FeIII]	0.27	0.30	0.27	0.32	-	0.28	0.26	0.29
5518	[ClIII]+OI	0.18	0.15	0.14	0.15	-	0.17	0.14	0.14
5538	[ClIII]	0.28	0.29	0.28	0.31	-	0.33	0.30	0.29
5755	[NII]	1.45	1.65	1.66	1.56	1.64	1.60	1.50	1.48
5876	HeI	20.8	21.3	21.2	20.4	21.5	16.9	19.1	19.4
6300	[OI]	6.82	5.91	6.73	6.35	6.70	6.38	5.88	6.10
6312	[SIII]	3.03	2.93	3.25	3.40	3.13	2.95	3.12	3.09
6364	[OI]	2.29	2.16	2.33	2.27	2.24	2.23	2.19	2.25
6563	H α	376	397	380	366	463	376	425	-
6584	[NII]	24.7	26.2	28.1	25.4	33.3	27.4	30.1	38.8
6678	HeI	5.52	5.75	5.69	5.41	6.56	5.11	5.31	-
6716	[SII]	0.86	0.96	0.92	0.88	1.14	0.77	1.04	-
6731	[SII]	1.85	1.95	1.91	1.85	2.34	1.71	1.89	-
7065	HeI	17.0	19.5	18.5	18.6	20.9	15.8	17.6	-
7136	[ArIII]	12.6	15.1	13.7	14.9	16.7	12.4	14.4	-
7170	[ArIV]	0.61	0.35	0.54	0.34	-	-	0.62	-
7237	[ArIV]	-	0.26	0.32	0.28	-	-	0.44	-
7281	HeI	-	1.63	1.39	1.31	1.18	-	1.70	-
7751	[ArIII]	-	-	3.12	-	-	-	-	-
9069	[SIII]	-	-	21.7	-	-	-	-	-
	$F(\text{H}\beta)$	3.14	2.87	3.24	3.05	3.04	3.24	3.25	3.33

Table 5: Continued

λ , Å	Ion	09.08.16	21.07.17	19.10.17	08.08.18	13.10.18	07.07.19	07.08.19	03.10.19
4102	H δ	18.2	19.6	19.7	19.9	17.4	19.3	19.8	19.4
4340	H γ	41.2	45.7	43.1	46.8	42.3	42.8	42	40
4363	[OIII]	30.6	32.2	30.8	32.5	29.0	32.6	35.5	32.7
4471	HeI	3.78	4.01	3.53	4.06	3.16	3.39	4.79	4.51
4712	HeI	0.68	0.83	0.73	0.77	0.77	0.92	1.05	0.9
4740	[ArIV]	0.32	0.36	0.32	0.29	0.30	0.44	0.49	0.46
4959	[OIII]	226	219	225	232	235	230	237	216
5007	[OIII]	-	671	670	-	715	-	726	658
5192	[ArIII]	0.11	0.13	-	0.13	0.10	0.10	0.15	0.09
5270	[FeIII]	0.27	0.26	-	0.27	0.26	0.26	0.27	0.31
5518	[ClIII]+OI	0.13	0.12	0.14	0.12	0.16	0.18	0.15	0.16
5538	[ClIII]	0.28	0.29	0.25	0.30	0.31	0.33	0.35	0.33
5755	[NII]	1.53	1.39	1.37	1.41	1.34	1.34	1.66	1.61
5876	HeI	19.1	18.9	16.6	18.7	18.9	18.1	19.4	19.7
6300	[OI]	6.25	6.43	5.33	5.77	6.01	5.8	7.16	6.94
6312	[SIII]	3.00	2.58	2.63	2.87	2.81	2.48	2.79	2.87
6364	[OI]	2.29	2.23	1.62	2.05	2.16	2.11	2.44	2.48
6563	H α	351:	438	321:	422	388	368	475	408
6584	[NII]	35.7	38.6	27.5	36.7	36.2	33.7	32.2	28.4
6678	HeI	5.03	5.33	4.12	4.88	5.01	4.92	5.48	5.75
6716	[SII]	1.02	0.85	0.73	0.75	0.84	0.88	0.97	0.97
6731	[SII]	1.77	1.93	1.50	1.79	1.84	1.82	2.08	2.20
7065	HeI	16.2	16.7	13.9	-	15.1	13.9	16.0	18.5
7136	[ArIII]	13.5	13.8	11.1	-	12.2	11.4	13.3	14.8
7170	[ArIV]	-	0.47	0.43	-	0.40	0.47	0.40	0.63
7237	[ArIV]	-	0.35	0.28	-	0.33	0.29	0.40	0.35
7281	HeI	1.10	1.80	1.29	-	1.68	1.43	1.57	1.74
7751	[ArIII]	-	3.63	2.17	-	3.12	2.85	3.46	3.86
9069	[SIII]	-	43.9	36.6	-	26.2	32.3	57.9	46.2
$F(\text{H}\beta)$	3.33	3.55	3.64	4.29	3.08	3.19	3.53	2.93	3.16

Table 6: Simulated physical conditions in the zone radiating $H\beta$, [OIII] $\lambda 4363, 4959$ for the 1970-2019 period.

	1970	1990	2003	2019
T_e , K	8000	11900	9740	7650
N_e , cm^{-3}	5.6(6)	5.3(6)	5.0(6)	5.14(6)
O^{2+}/H^+	4.2(-3)	6.5(-4)	2.18(-3)	6.0(-3)
$F(\lambda 5876)/F(H\beta)$	0.19	0.22	0.20	0.19
T_e , K	10000	16700	12800	9440
N_e , cm^{-3}	2.16(6)	2.3(6)	2.05(6)	2.01(6)
O^{2+}/H^+	7.7(-4)	1.27(-4)	2.4(-4)	1.13(-3)
$F(\lambda 5876)/F(H\beta)$	0.20	0.29	0.23	0.20
T_e , K	12000	22600	16150	12220
N_e , cm^{-3}	1.18(6)	1.4(6)	1.17(6)	1.08(6)
O^{2+}/H^+	2.7(-4)	4.6(-5)	1.5(-4)	4.0(-4)
$F(\lambda 5876)/F(H\beta)$	0.22	0.36	0.28	0.21